Platinum surface instabilities and their impact in electrochemistry

Valls Mascaro, F.

A Supplementary Information on Chapter 2

A.1 Chemical Potential of Adatoms

The total chemical potential of the surface μ_s is the sum of all the contributions from the different surface species: adatoms, step adatoms, kink atoms, step atoms, etc:

$$\mu_s = \mu_{ad} + \mu_{step\,adatom} + \mu_{kink} + \mu_{step} + ... \tag{A.1}$$

In thermodynamic equilibrium, μ_s is equal to the equilibrium chemical potential, and the local chemical potentials of each of the surface entities described above pursue to balance their difference. Based on Fick's laws, this is achieved by e.g. transport of atoms from a kink site to the terrace, thereby increasing the adatom concentration.

In this work, we are interested in calculating the equilibrium adatom concentration at different electrode potentials, and comparing them to the actual adatom concentrations to know whether nucleation is thermodynamically favorable. Therefore, we are interested specifically in the term μ_{ad}.

In the Adatom Lattice Gas model, the adatoms reside in defined specific sites on the surface, thus forming a lattice gas. If we assume that the adatoms in the lattice gas do not interact between each other, then μ_{ad} can be derived from Fermi-statistics, yielding [1]:

$$\mu_{ad} = \mu_0 + k_B\,T\,\ln(\tfrac{\theta_{ad}}{1-\theta_{ad}}) \tag{A.2}$$

where μ_0 is the ground state energy of an adatom, which is equal to the formation energy of an adatom (E_{ad}) referenced to the energy of a kink, k_B is the Boltzmann constant, and T is the temperature. The term $k_B\,\ln(\frac{\theta_{ad}}{1-\theta_{ad}})$ describes the entropy. We could also include attractive/repulsive interactions by adding the term $W(\theta_{ad})$ to eq. A.2. However, it has been shown with STM on Cu(111) that this interaction energy is in the order of meV at low adatom concentrations, and therefore one typically neglects this term [2].

At thermodynamic equilibrium, $\mu_{ad} = \mu_{kink}$, and therefore we can solve eq. A.2 for the equilibrium adatom concentration ($\theta_{eq,ad}$):

$$\theta_{eq,ad} = \frac{exp(\frac{-E_{ad}}{k_B T})}{1+exp(\frac{-E_{ad}}{k_B T})} \tag{A.3}$$

At low adatom coverages, the entropy term in eq. A.2 can be approximated to

$$\frac{\partial S}{\partial N_{ad}} = k_B \ln(\frac{\theta_{ad}}{1-\theta_{ad}}) \approx k_B \ln(\theta_{ad}) \tag{A.4}$$

and hence

$$\mu_{ad} \approx \mu_0 + k_B T \ln(\theta_{ad}) \tag{A.5}$$

The adatom concentration is then described by the well known Boltzmann equation:

$$\theta_{ad} = exp(\frac{-E_{ad}}{k_B T}) \tag{A.6}$$

In Fig. A.1, we evaluate the relative error made at different potentials, thus different PtO_2-adatom equilibrium concentrations ($\theta_{eq,ad}$), when taking the approximation in the entropy term. We define the error as:

$$Error = \left|\theta_{eq,ad}\,(eq.\,A.3) - \theta_{eq,ad}\,(eq.\,A.6)\right| \tag{A.7}$$

and the relative error as:

$$Relative\,Error = \frac{\left|\theta_{eq,ad}\,(eq.\,A.3) - \theta_{eq,ad}\,(eq.\,A.6)\right|}{\theta_{eq,ad}\,(eq.\,A.6)} \tag{A.8}$$

Note that this relative error is very low ($< 6\cdot10^{-4}$) at potentials up to 0.85 V. Therefore, the Boltzmann equation describes the equilibrium adatom concentration sufficiently correct up to 0.85 V, but we need the full entropy expression to calculate $\theta_{eq,ad}$ at higher potentials.

A.2 Adatom Latice Gas Model

As explained above, in the Adatom Lattice Gas model the adatoms are adsorbed at defined surface sites on the terrace. The entropy S is given by [3, 4]:

$$S = k_B\, ln(\Omega) \tag{A.9}$$

where Ω is the number of different configurations in which the adatoms can be placed. For N_{ad} number of adatoms on a terrace with N_s number of sites,

$$\Omega = \frac{N_s!}{N_{ad}!\,(N_s - N_{ad})!} \tag{A.10}$$

and by using the Stirling approximation $ln(n!) = n\,ln(n) - n$,

$$\Omega = (N_s\,ln(N_s) - N_s) - (N_{ad}\,ln(N_{ad}) - N_{ad}) - (N_s - N_{ad})\,ln(N_s - N_{ad}) + (N_s - N_{ad}) \tag{A.11}$$

Solving the partial derivative on S in eq. A.9 leads to:

$$-T\frac{\partial S}{\partial N_{ad}} = -k_B\, T\, ln(\frac{N_s - N_{ad}}{N_{ad}}) \tag{A.12}$$

Defining then the adatom coverage as $\theta_{ad} = \frac{N_{ad}}{N_s}$, we finally obtain

$$-T\frac{\partial S}{\partial N_{ad}} = -k_B\, T\, ln(\frac{\theta_{ad}}{1-\theta_{ad}}) \tag{A.13}$$

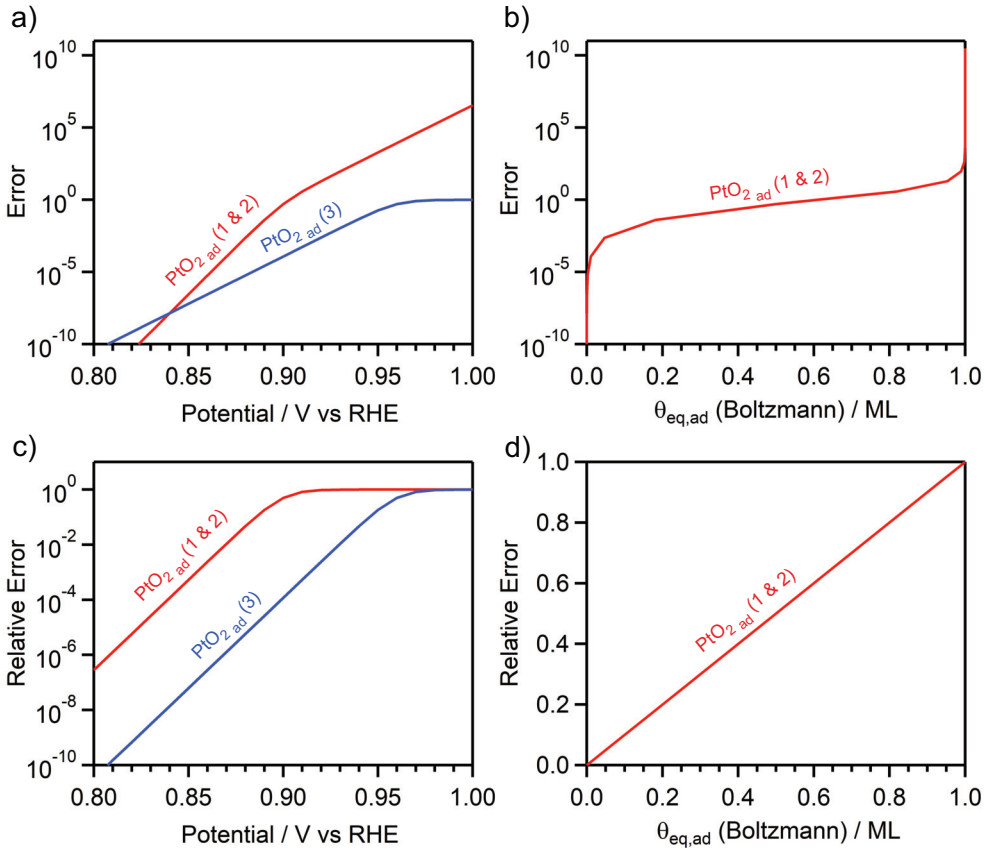

Figure A.1: Error made when calculating the PtO_2-adatom equilibrium concentrations with the Boltzmann approximation in the entropy term. **(a)** and **(b)** are the absolute erors, versus potential and coverage (calculated with eq. A.6), respectively, while **(c)** and **(d)** are the relative errors. In **(b)** and **(d)**, we show only the error for $\theta_{eq,PtO_2,ad}$ (1&2), as the error for $\theta_{eq,PtO_2,ad}$ (3), when represented versus coverage, is exactly the same.

Realize that this entropy term is also included in the Langmuir isotherm. However, there is one major difference between the Adatom Lattice Gas model and the Langmuir isotherm: while the isotherm considers atoms/molecules from a liquid or gas phase adsorbing on a solid phase, in the Adatom Lattice Gas model the atoms adsorbed on the surface are the adatoms, which are formed from kinks at the steps. As a kink site repeats itself after removing a kink atom (i.e. thus forming an adatom), the reservoir of kinks is infinite.

A.3 Energy of Oxygen Adsorption as Function of Coverage

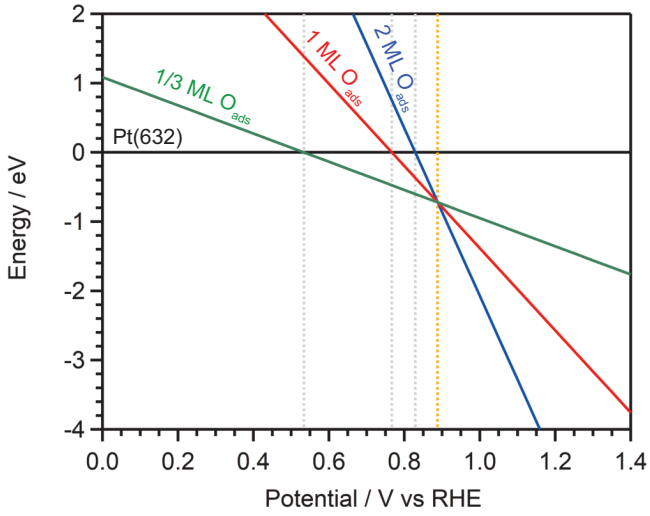

Figure A.2: Gibbs Free Energy for Oxygen Adsorption as a Function of Oxygen Coverage along the Step. The reference used is the energy of a Pt(632) surface, in black. The dotted gray lines indicate the potentials at which each of the oxygen adsorption energies considered crosses zero, while the yellow line indicates the potential at which the three adsorption energies are equal.

A.4 STM Images and Statistical Analysis of the Dendritic Islands

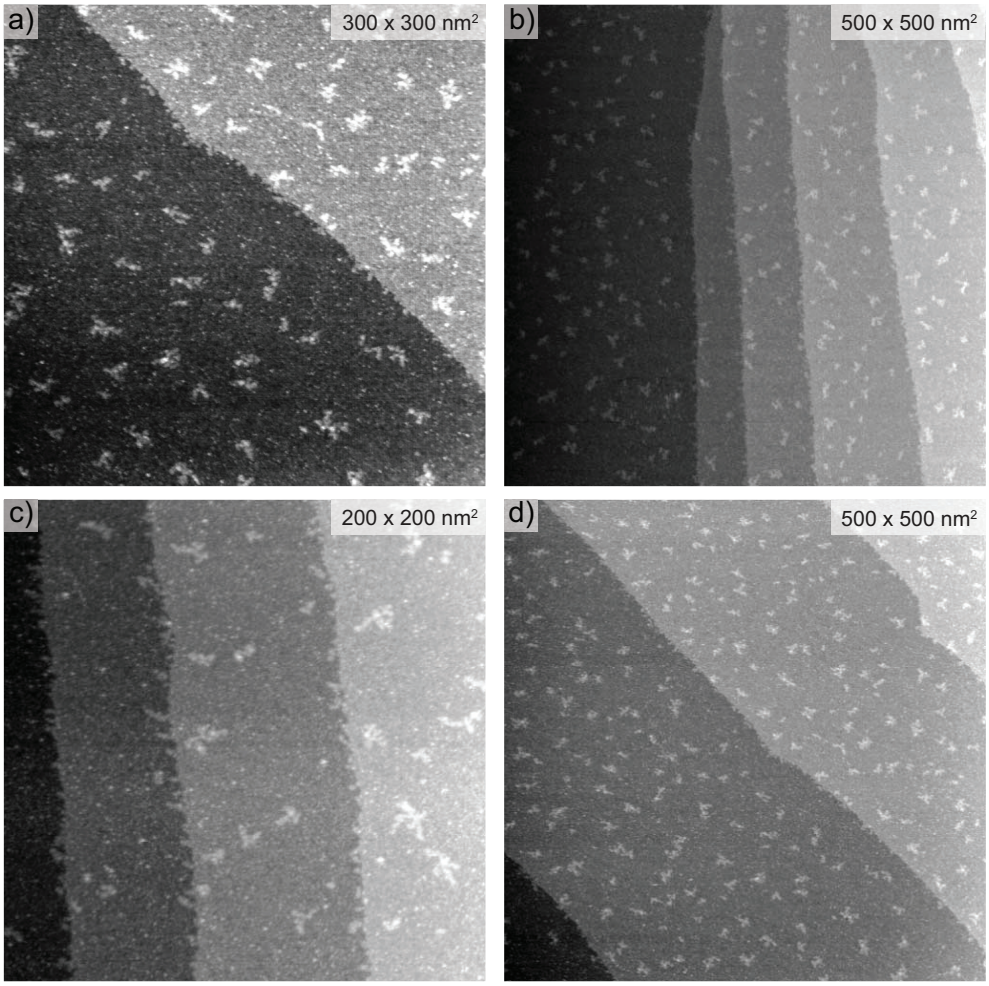

Figure A.3: Vacuum-STM Images of Dendritic Islands on Pt(111). The islands were formed after a potential step from 1.0 V to 1.3 V, where the potential was hold for 10 s, and then stepping back to 1.0 V before finally sweeping to 0.05 V at 50 mV/s. The four images were used to perform the statistical analysis of the island shape that is described in the main text for the measurement in vacuum. The images are reproduced with permission from T. Maagaard.

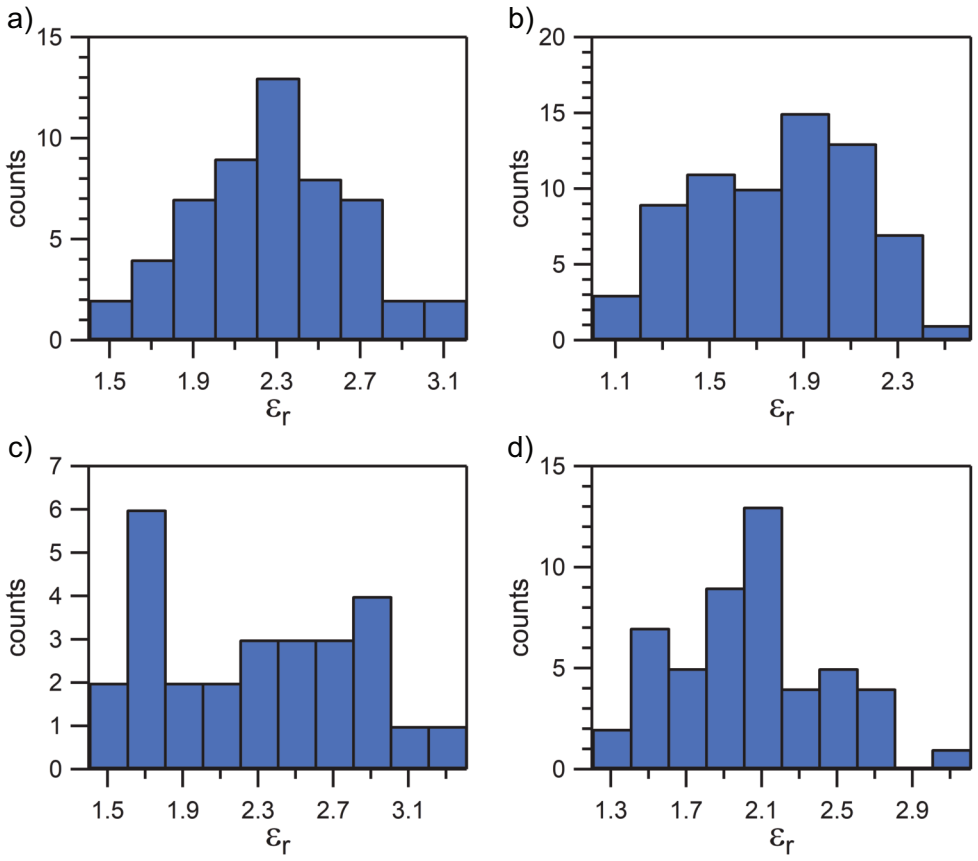

Figure A.4: Statistical Distribution of ϵ_r for the Best Estimate of the Island Shapes Measured in Vacuum. We obtained each of the histograms from analyzing the islands in the according images presented in Fig. A.3, e.g. Fig. A.4a was obtained from analyzing the islands in Fig. A.3a. Merging these four histograms into one results in the statistical distribution shown in Fig. 2.8a

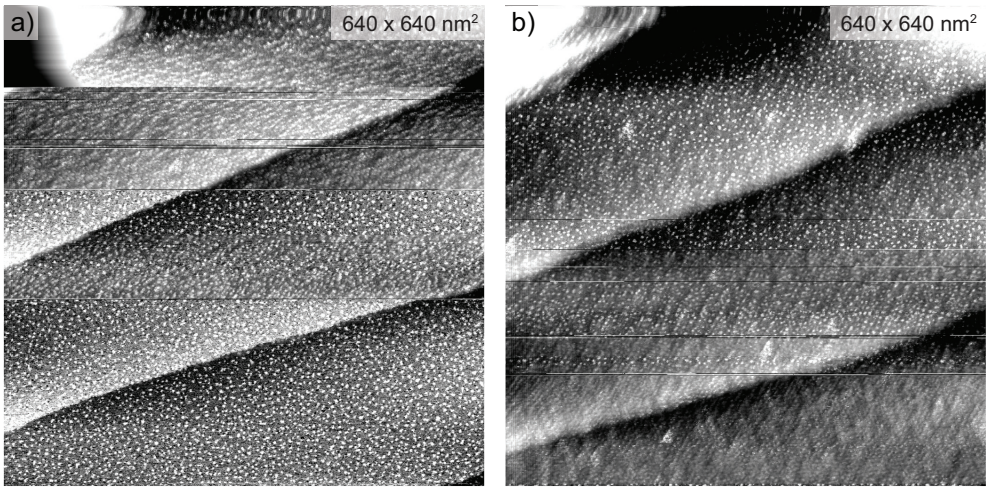

Figure A.5: EC-STM Images of Dendritic Islands on Pt(111). The islands were formed after holding the potential at 1.35 V during 200 s, and then reducing to 0.3 V with 25 mV/s. The two images were used to perform the statistical analysis of the island shape that is described in the main text for the measurement in electrolyte.

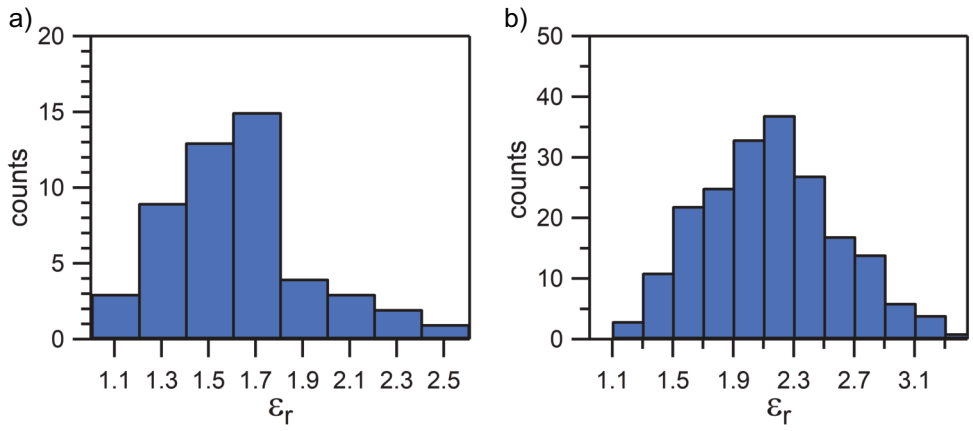

Figure A.6: Statistical Distribution of ϵ_r for the Best Estimate of the Island Shapes Measured in the Electrolyte. We obtained each of the histograms from analyzing the islands in the according images presented in Fig. A.5, e. g. Fig. A.6a was obtained from analyzing the islands in Fig. A.5a. Merging these two histograms into one results in the statistical distribution shown in Fig. 2.8b.

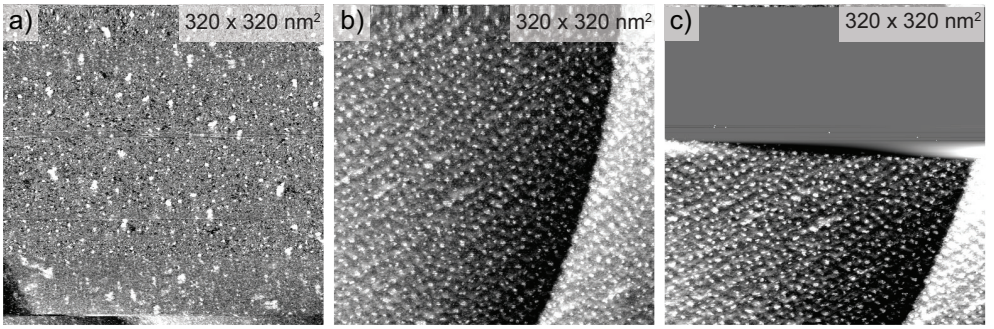

Figure A.7: EC-STM Images of Dendritic Islands Formed on Pt(111) upon Oxidation-Reduction Cycling. The islands were formed after 1 **(a)**, 6 **(b)**, and 7 **(c)** oxidation-reduction cycles from 0.06 V to 1.35 V at 50 mV/s. The three images were used to perform the statistical analysis of the island shape that results in the histograms shown in Fig. 2.10.

References

[1] H. Ibach, *Physics of Surfaces and Interfaces*, Springer, Amsterdam (2006).

[2] J. Repp, F. Moresco, G. Meyer, K. H. Rieder, P. Hyldgaard, and M. Persson, *Phys. Rev. Lett.*, **85**(14), 2981 (2000).

[3] T. Hill, *An Introduction to Statistical Thermodynamics*, Addison-Wesley Publishing Company, Reading (1960).

[4] A. Saedi, and M. J. Rost, *Nat. Commun.*, **7**, 10733 (2015).

B Supplementary Information on Chapter 3

B.1 EC-STM Image Processing

Figure B.1a shows a 48x48 nm^2 raw EC-STM image of a Pt(554) surface, obtained at U_s = 0.1 V and U_t = 0.15 V. Due to the tilt of the sample, which even pushes the contrast out of the color scale at the upper left and the lower right of the image, the atomic steps are barely visible. Therefore, we performed a planar background subtraction of the image, which enhances the contrast on the surface features (Fig. B.1b). However, this image is inadequate for a proper analysis, as it does not reflect the natural tilt of the stepped surface. We need to rotate the image along the axis parallel to the step direction until the steps have the expected mono-atomic step height (2.27 Å), which is similar to aligning the terraces fully in-plane without any slope. The height line (in orange) should, in this case, reveal a series of descending and flat sections, resembling a staircase. Figure B.1c shows the same height line for three different rotation angles. For each of them, we measured the average step height, which we plotted in Fig. B.1d. Finally, we determined the correct rotation angle from the linear regression shown in the graph, setting X = 2.27 Å. This delivers α = 5.68°, which is very close to the miscut angle of Pt(554) with respect to the (111) plane of 5.77°. However, this does not necessarily have to be the case for all images or height lines, as the surface can present, locally, areas with more or less tilt, i. e. step density. In general, this also depends on the mounting of the sample in the sample holder as well as the different lengths of the micrometer screws that are used for the coarse approach. To avoid an inaccurate analysis, we performed the above described procedure for all height lines, and not only for Pt(554), but also for Pt(553). However, as the latter has bunched steps with higher multiplicity, we took this into account by expecting step heights close to 2.27 Å, 4.54 Å, or 6.81 Å. Note that the steps are not vertical in Fig. B.1c, even not with correct rotation, which is due to the tip convolution with the step structure.

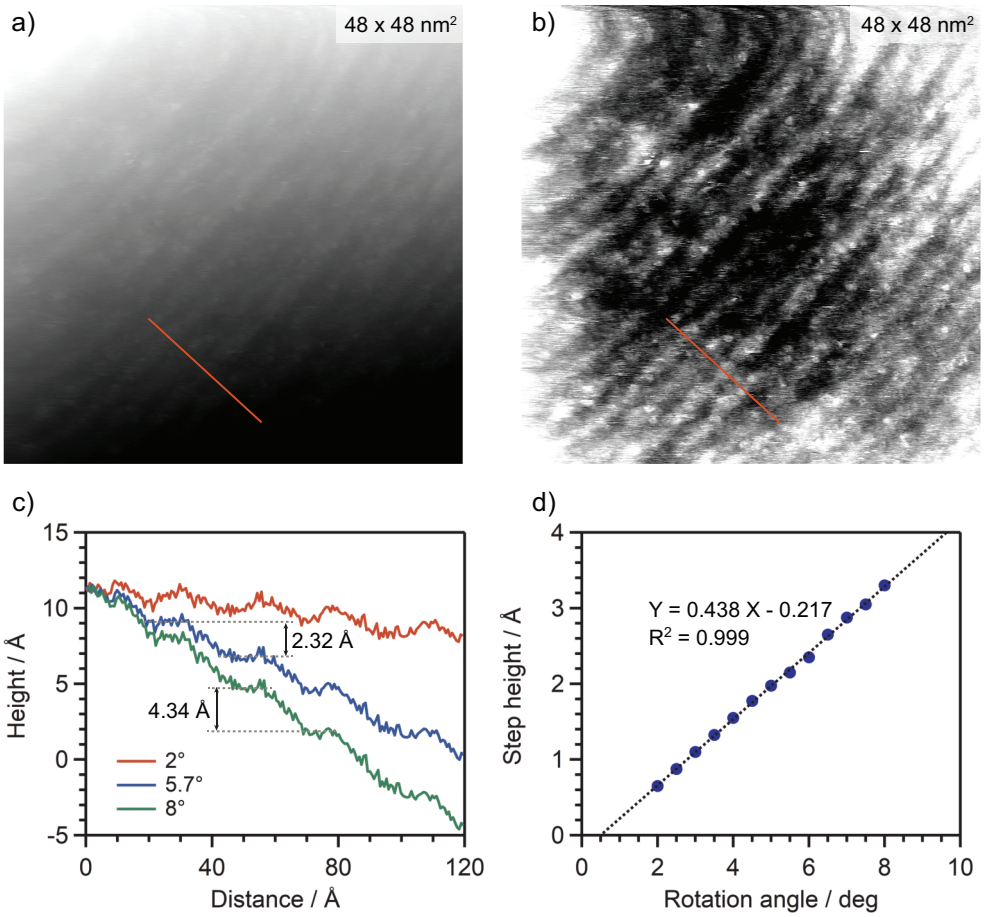

Figure B.1: EC-STM Image Processing to Extract Accurate Step Heights. **(a)** Raw EC-STM image (48x48 nm^2) of a Pt(554) surface, obtained at U_s = 0.1 V and U_t = 0.15 V. **(b)** Same image after planar background subtraction enhancing the contrast. **(c)** Height lines at the indicated position in (a) and (b) with different rotation angles: 2°, 5.7°, and 8°. **(d)** Average step height versus the rotation angle of the height line to determine the best correction angle.

B.2 EC-STM Images of Pt(554) and Pt(553)

Figures B.2 and B.3 show all the EC-STM images used for the analysis of the terrace width and step height distributions. In order to enhance the contrast of the surface features, here we show the images after applying a line-by-line background subtraction. For the actual analysis, we processed the images as explained above.

The distortion at the top and sides on (some of) the EC-STM images is due to the creep of the STM piezo-tube at the beginning of every new frame or scan line. In our analysis we avoided these distorted areas, as well as the areas that show contamination.

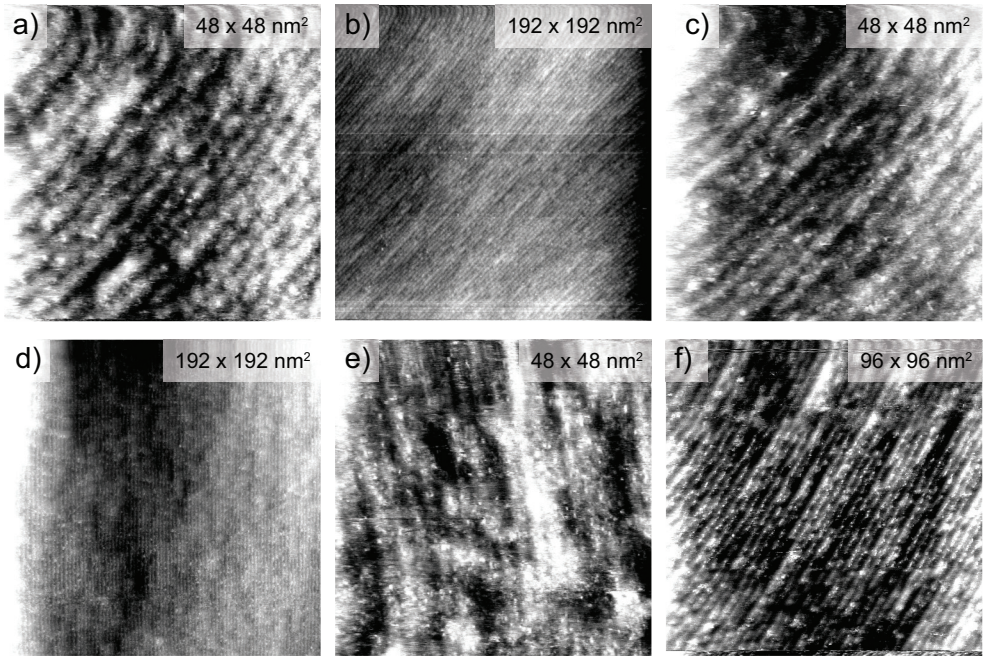

Figure B.2: EC-STM Images of Pt(554). We recorded all the images at $U_s = 0.1$ V and either $U_t = 0.15$ V or $U_t = 0.20$ V, with tunneling currents in the range of 300 pA. The corresponding image sizes are indicated.

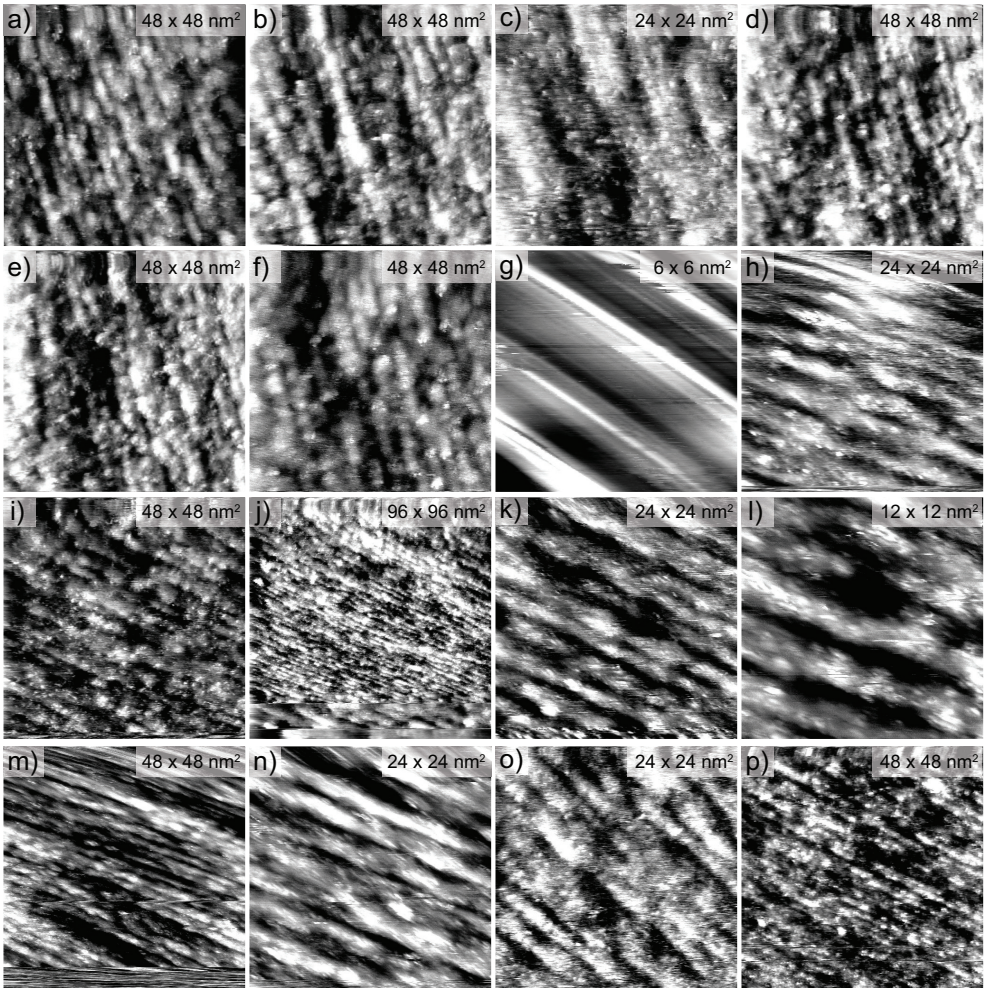

Figure B.3: EC-STM Images of Pt(553). We recorded all the images at U_s = 0.1 V and either U_t = 0.15 V or U_t = 0.20 V, except for **(j)** and **(l)**, which we recorded at U_s = 0.4 V and U_t = 0.45 V. The tunneling currents were in the range of 300-700 pA except for **(g)**, which was recorded at 1200 pA. The corresponding image sizes are indicated.

B.3 Terrace Width and Step Height Distributions on Pt(553)

Figures B.4 and B.5 show the terrace width and step height distributions for Pt(553) from EC-STM measurements performed on different days, and thus different sample preparation. All the histograms show mainly three different peaks, corresponding to single steps, double steps, and triple steps, as explained in the main article. This proves that the Pt(553) surface, prepared with the flame-annealing method followed by cooling in an Ar-H_2 atmosphere, is always bunched.

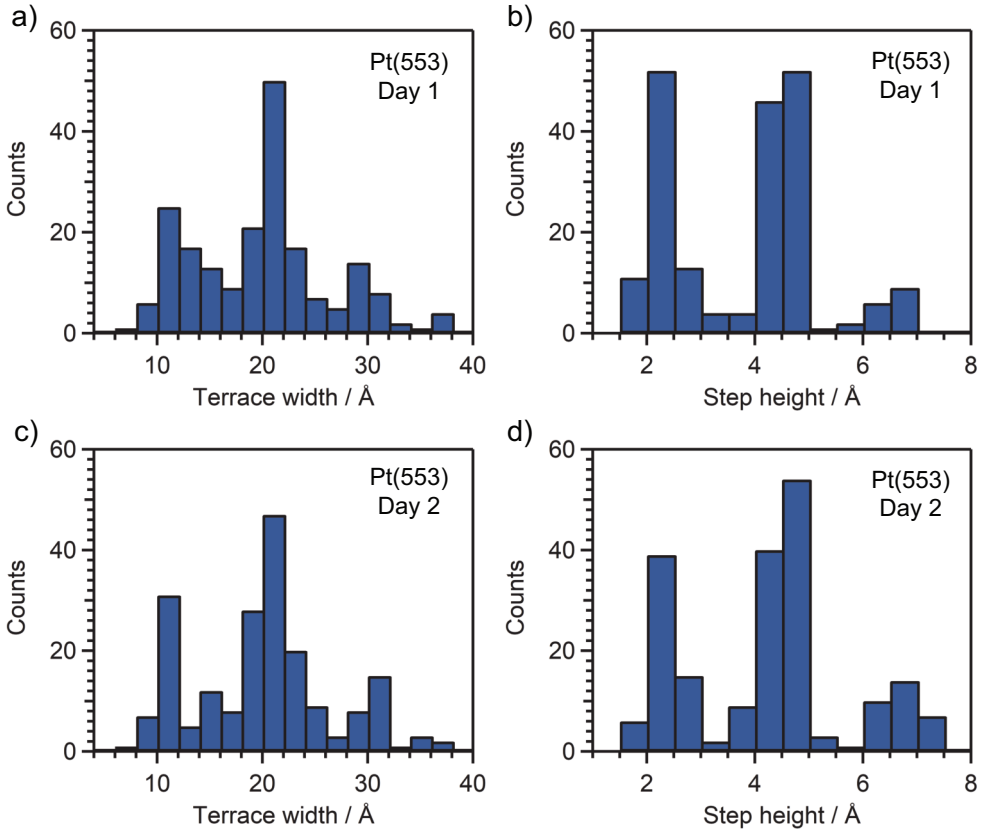

Figure B.4: Terrace Width and Step Height Distributions for Pt(553) on different days. I. Day 1 ((**a**) and (**b**)) corresponds to the EC-STM images **(a)**-**(f)** in Fig. B.3, Day 2 ((**c**) and (**d**)) to images **(h)**-**(j)**.

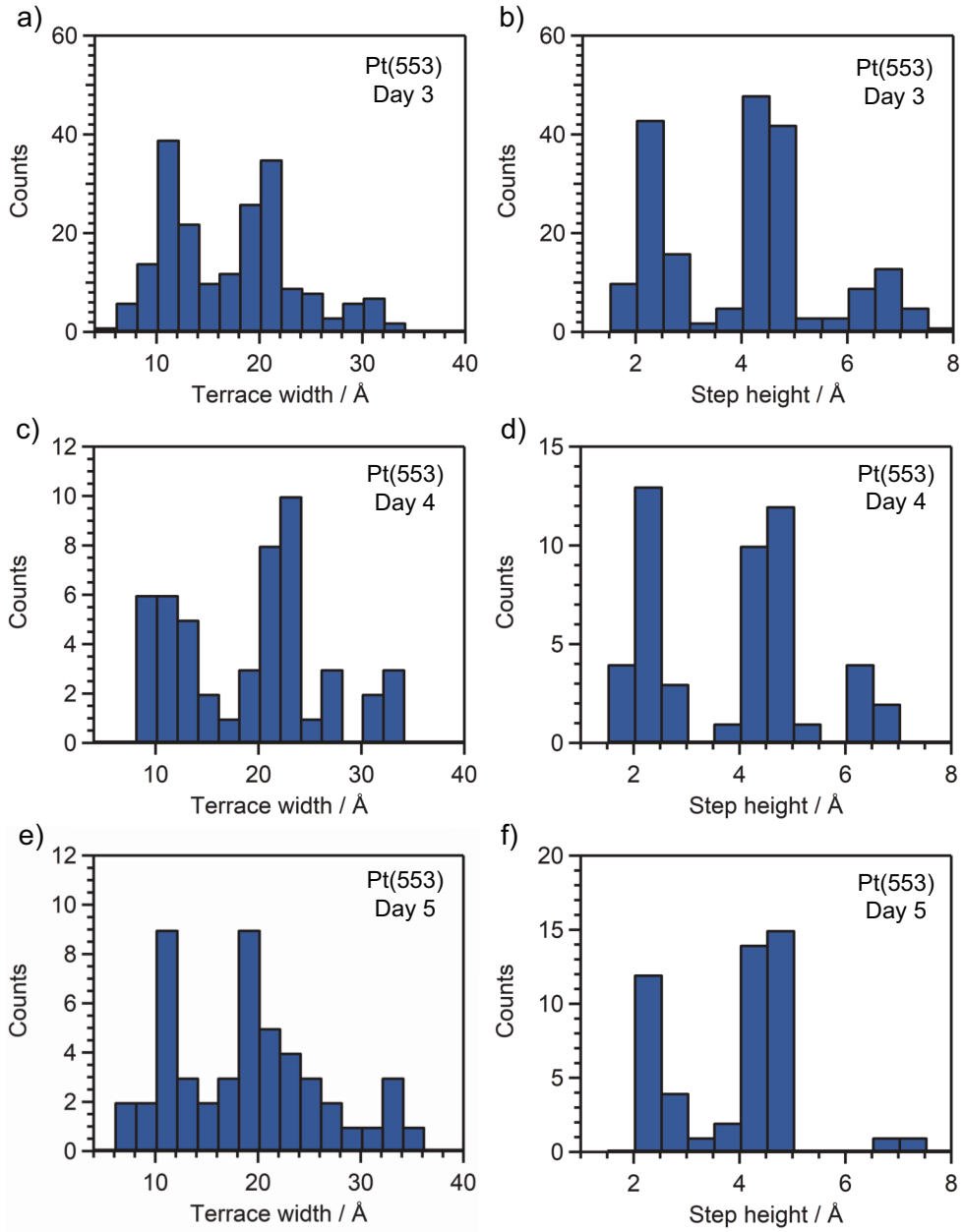

Figure B.5: Terrace Width and Step Height Distributions for Pt(553) on different days. II. Day 3 ((**a**) and (**b**)) corresponds to the EC-STM images shown in Fig. B.3 **(k)**-**(n)**, Day 4 ((**c**) and **(d)**) to Fig. B.3 **(o)**, and Day 5 ((**e**) and **(f)**) to the one shown in Fig. B.3 **(p)**.

B.4 Effect of Potential and Hydrogen Coverage

Fig. B.6 shows one of the EC-STM images on Pt(553) recorded at a sample potential of 0.4 V after holding this potential for 60 minutes (previously it was 0.1 V). The presence of double steps is evident from the height line. As explained in the main manuscript, in the time span evaluated we did not observe a different surface structure when changing the applied potential.

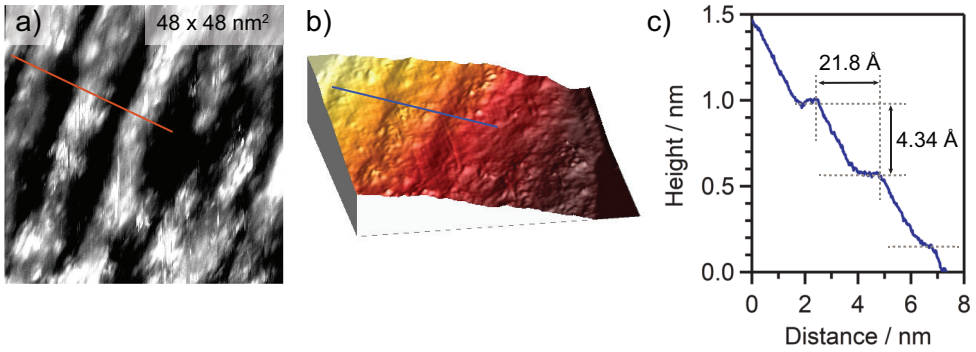

Figure B.6: EC-STM Image of Pt(553) at 0.4 V. (a) 2D Image after background subtraction and its corresponding 3D representation **(b)**, recorded at $U_s = 0.4$ V and $U_t = 0.45$ V, with a tunneling current in the range of 300 pA. Both images are 48x48 nm^2. **(c)** Height line showing double steps.

B.5 Calculation of the Step-Step Interaction

The step interaction coefficient B_{step} must take into account the entropic repulsion as well as the electrostatic and elastic interactions between neighboring steps. As the latter two go with $U = A/L^2$, where U is the energy per length between steps and A the magnitude of both energetic interactions, B_{step} is given by [1]:

$$B_{step}(T) = \frac{(\pi k_B T)^2 a}{24 \widetilde{\beta}(T)} \left[1 + \sqrt{1 + \frac{4 A \widetilde{\beta}(T)}{(k_B T)^2}} \right]^2 \tag{B.1}$$

where $\widetilde{\beta}$ is the step stiffness, which can be calculated from [2]:

$$\widetilde{\beta}(T) = \frac{k_B T a}{b^2(T)} \tag{B.2}$$

with b being the step diffusivity, which can be obtained from an STM statistical analysis of the mean-squared displacement of an isolated step perpendicular to the step edge. Alternatively, we can calculate b from the kink formation energy f_{kink}, as [2]:

$$b^2(T) = \frac{2 d\, e^{-f_{kink}/(k_B T)}}{1 + 2\, e^{-f_{kink}/(k_B T)}} \tag{B.3}$$

where d is the unit vector perpendicular to the step edge. Thus, with equations B.1-3 and taking $A = 2.4$ eV Å from Ref. [1], we can easily determine B_{step} at any given temperature.

In order to obtain the interaction coefficient of double steps, $B_{double\,step}$, we first need to estimate $A_{double\,step}$. As A goes, in general, with the square of the electric (or elastic) dipole moment ($A \propto p_z^2$) [3,4], we can calculate $A_{double\,step}$ from the ratio:

$$\frac{A_{double\,step}}{A_{single\,step}} = \left[\frac{p_{z,double\,step}}{p_{z,single\,step}}\right]^2 \tag{B.4}$$

As we extracted $p_{z,double\,step}$ from Fig. 3.5 in the main manuscript, $A_{double\,step}$ naturally follows, and we can finally use eq. B.1-3 to calculate $B_{double\,step}$.

B.6 Temperature Effect on Step Bunching

The variation of temperature has an effect on the step free energy as well as on the entropic term of the step-step interaction, and hence ultimately on the total free energy of the surface. Figure B.7 shows the free energy ratios between a surface with double steps and one with single steps at different temperatures. As evident from this graph, decreasing the temperature results in an earlier onset for step bunching, from $n = 8$ at $T = 1300$ K to $n = 15$ at $T = 900$ K. The main reason for this is that at lower temperature there is a reduced concentration of thermally-activated kinks that decrease the free energy of the single steps (i. e. on double steps the concentration of thermally-activated kinks is anyhow much smaller due to the higher kink formation energy). This leads to a higher step stiffness and, therefore, single steps are more prone to bunching at lower temperatures.

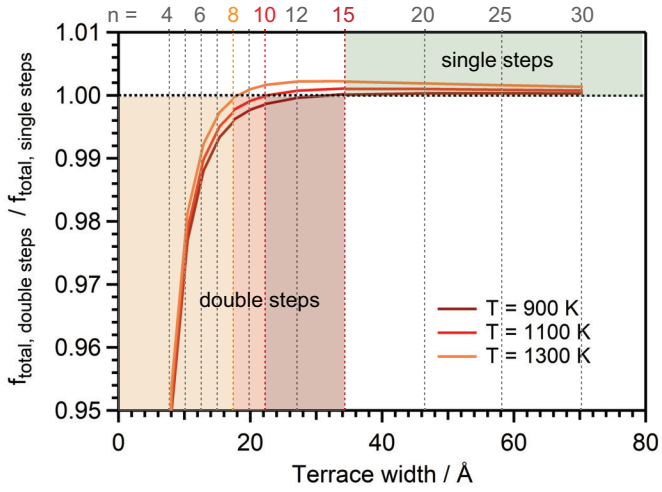

Figure B.7: Effect of Temperature on Step Bunching. Surface energy ratio between configurations with double and with single steps at different temperatures. The vertical colored lines indicate the onset of step bunching (where the curves cross the ratio equal to one) at each of the temperatures evaluated. The regions with stable single steps and stable double steps are indicated.

B.7 Effect of Step Bunching on the Hydrogen Adsorption

In Fig. 3.5 in the main text, we showed that Pt(553) and Pt(221), two stepped surfaces that have bunched steps, present an extra voltammetric peak in the hydrogen desorption region. We assigned this peak to hydrogen desorption and its (partial) replacement with hydroxide at bunched steps, as we discussed in depth in Chapter 4. However, step bunching has also a slight influence on the adsorption/desorption energetics on single steps, as it changes the step separation and thus the repulsion. Figure B.5 shows, for each surface studied, the potential value at the center of the hydrogen single-step peak (E_{H-step}), which is closely related to the adsorption/desorption energy [5]. From Pt(111), which has a very small amount of steps, to Pt(554) E_{H-step} increases, which could be caused by the raising interaction between steps as the terrace width decreases [3, 4, 6, 7]. However, Pt(775) does no longer follow the trend, and jumps back to a much a lower E_{H-step}. This suggests that Pt(775) has also step bunches, although, as we discuss in the main text, the density of single steps must be much higher.

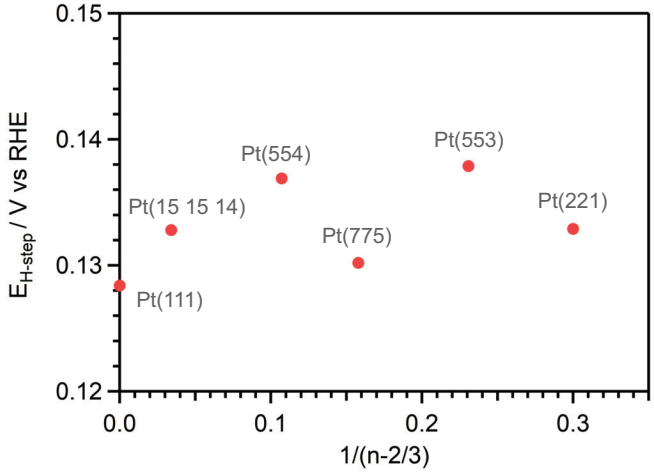

Figure B.8: Potential of the H-step Peak versus the Step Density. The data points correspond to the potential values at the the center of the respective single step peaks in the hydrogen desorption region, which we show in Fig. 3.5 in the main text.

B.8 Stability of Stepped Platinum Surfaces: Literature Study

Although we only performed EC-STM measurements on Pt(554) and Pt(553), we can deduce whether other stepped platinum surfaces are stable from their electrochemical behavior. As we discussed in the main article, stepped surfaces that undergo step bunching present an unexpected E_{pztc} and ORR activity. However, other electrochemical reactions such as CO Oxidation, the Hydrogen Oxidation Reaction (HOR), Hydrogen Peroxide Reduction, and Nitrate Reduction are also affected. Based on this, in Tables B.1-B.3 we assessed the stability of many stepped platinum surfaces in the [1 -1 0], [0 1 -1], and [0 0 1] zones, respectively, all prepared with the flame-annealing method.

(111)x(111)	n	Stable?	Measurements
(15 15 14)	30	Yes	ORR [8], CO Oxidation [9]
(10 10 9)	20	Yes	STM [10]
(554)	10	Yes	ORR [11], H_2O_2 Red. [12], NO_3^- Red. [13], CO Ox. [9], E_{pztc} [14, 15]
(997)	9	Yes	ORR [16], HOR [17]
(775)	7	No	ORR [11, 16], H_2O_2 Ox. [12], NO_3^- Red.* [13], E_{pztc} [14, 15]
(332)	6	No	ORR [11], NO_3^- Red. [13], E_{pztc} [15]
(553)	5	No	H_2O_2 Red. [18], NO_3^- Red. [13], CO Ox. [9], HOR [17], E_{pztc} [14, 15]
(221)	4	No	ORR [11, 16], H_2O_2 Red. [12], NO_3^- Red. [13], E_{pztc} [14, 15]
(331)	3	No	SXRS [19], ORR [11, 16], H_2O_2 Red. [12, 18], NO_3^- Red. [13], E_{pztc} [14, 15]
(110)x(111)	n	Stable?	Measurements
(551)	3	No	CV H_{upd} [20]
(991)	5	No	CV H_{upd} [20]
(19 19 1)	10	No	CV H_{upd} [20]

Table B.1: Stability of Stepped Platinum Surfaces in the [1 -1 0] Zone. This comprises (111) vicinal surfaces with (111) steps and (110) vicinals with (111) steps. The Nitrate Reduction measurement on Pt(775) (marked with an asterisk) suggests that this surface is stable, while the other measurements show the contrary. For all the other surfaces, there is a total agreement between different techniques.

(111)x(100)	n	Stable?	Measurements
(15 14 14)	29	Yes	H_2O_2 Red. [12]
(11 10 10)	21	Yes	STM [10]
(15 13 13)	14	Yes	ORR [21]
(11 9 9)	10	Yes	E_{pztc} [22]
(544)	9	Yes	ORR [21], H_2O_2 Red. [12], CV H_{upd} [23]
(755)	6	No	ORR [11, 21], H_2O_2 Red. [12, 18], E_{pztc} [22], CV H_{upd} [23]
(322)	5	No	H_2O_2 Red. [12, 18]
(533)	4	No	ORR [11, 21], E_{pztc} [22], CV H_{upd} [23]
(211)	3	No	ORR [11, 21], H_2O_2 Red. [12, 18], HOR [24], E_{pztc} [22], CV H_{upd} [23]
(311)	2	No	SXRS [19, 25], ORR [11], HOR [24], E_{pztc} [22], CV H_{upd} [23]
(100)x(111)	n	Stable?	Measurements
(511)	3	No	SXRS [19]
(771)	4	Yes	ORR [11], E_{pztc} [26]
(11 1 1)	6	Yes	E_{pztc} [26]
(15 1 1)	8	Yes	ORR [11]
(19 1 1)	10	Yes	E_{pztc} [26]
(29 1 1)	15	Yes	STM [26], E_{pztc} [26]

Table B.2: Stability of Stepped Platinum Surfaces in the [0 1 -1] Zone. This comprises (111) vicinal surfaces with (100) steps and (100) vicinals with (111) steps.

(100)x(110)	n	Stable?	Measurements
(20 1 0)	20	Yes	Co Ox. [27]
(10 1 0)	10	Yes	Co Ox. [27]
(710)	7	Yes	Co Ox. [27]
(510)	5	No	Co Ox. [27]
(310)	3	No	SXRS [28], Co Ox. [27]
(210)	2	No	Co Ox. [27]
(110)x(100)	n	Stable?	Measurements
(320)	3	No	E_{pztc} [29]
(430)	4	No	E_{pztc} [29]
(540)	5	No	E_{pztc} [29]
(760)	7	No	E_{pztc} [29]
(10 9 0)	10	No	E_{pztc} [29]

Table B.3: Stability of Stepped Platinum Surfaces in the [0 0 1] Zone. This comprises (100) vicinal surfaces with (110) steps and (110) vicinals with (100) steps.

References

[1] H. Jeong, E. D. Williams, *Surf. Sci. Rep.*, **34**, 171 (1999).

[2] H. Ibach, *Physics of Surfaces and Interfaces*, Springer, Amsterdam (2006).

[3] C. Jayaprakash, C. Rottman, and W. F. Saam, *Phys. Rev. B*, **30**, 6549 (1984).

[4] V. I. Marchenko and A. Ya. Parshin, *Sov. Phys. JETP*, **52**, 129 (1980).

[5] A. J. Bard and L. R. Faulkner, *Electrochemical Methods: Fundamentals and Applications*, 2nd ed., Wiley, New York (2001).

[6] K. H. Lau and W. Kohn, *Surf. Sci.*, **65**, 607 (1977).

[7] R. Smoluchowski, *Phys. Rev.*, **60**, 661 (1941).

[8] A. M. Gómez-Marín and J. M. Feliu, *Catal. Today*, **244**, 172 (2015).

[9] N. P. Lebedeva, M. T. M. Koper, J. M. Feliu, and R. A. van Santen, *J. Phys. Chem.*, **106**, 12938 (2002).

[10] E. Herrero, J. M. Orts, A. Aldaz, and J. M. Feliu, *Surf. Sci.*, **440**, 259 (1999).

[11] R. Rizo, E. Herrero, and J. M. Feliu, *Phys. Chem. Chem. Phys.*, **15**, 15416 (2013).

[12] R. Rizo, J. M. Feliu, and E. Herrero, *J. Catal.*, **398**, 123 (2021).

[13] S. Taguchi and J. M. Feliu, *Electrochim. Acta*, **52**, 6023 (2007).

[14] V. Climent, R. Gómez, and J. M. Feliu, *Electrochim. Acta*, **45**, 629 (1999).

[15] V. Climent, G. A. Attard, and J. M. Feliu, *J. Electroanal. Chem.*, **532**, 67 (2002).

[16] A. Kuzume, E. Herrero, and J. M. Feliu, *J. Electroanal. Chem.*, **599**, 333 (2007).

[17] N. Hoshi, Y. Asaumi, M. Nakamura, K. Mikita, and R. Kajiwara, *J. Phys. Chem. C*, **113**, 16843 (2009).

[18] E. Sitta, A. M. Gómez-Marín, A. Aldaz, and J. M. Feliu, *Electrochem. Commun.*, **33**, 39 (2013).

[19] N. Hoshi, M. Nakamura, O. Sakata, A. Nakahara, K. Naito, and H. Ogata, *Langmuir*, **27**, 4236 (2011).

[20] J. Souza-Garcia, V. Climent, and J. M. Feliu, *Electrochem. Commun.*, **11**, 1515 (2009).

[21] M. D. Maciá, J. M. Campina, E. Herrero, and J. M. Feliu, *J. Electroanal. Chem.*, **564**, 141 (2004).

[22] R. Gómez, V. Climent, J. M. Feliu, and M. J. Weaver, *J. Phys. Chem. B*, **104**, 597 (2000).

[23] N. Garcá-Aráez, V. Climent, and J. M. Feliu, *Electrochim. Acta*, **54**, 966 (2009).

[24] R. Kajiwara, Y. Asaumi, M. Nakamura, and N. Hoshi, *J. Elecroanal. Chem.*, **657**, 61 (2011).

[25] A. Nakahara, M. Nakamura, K. Sumitani, O. Sakata, and N. Hoshi, *Langmuir*, **23**, 10879 (2007).

[26] K. Domke, E. Herrero, A. Rodes, and J. M. Feliu, *J. Electroanal. Chem.*, **552**, 115 (2003).

[27] F. J. Vidal-Iglesias, J. Solla-Gullón, J. M. Campina, E. Herrero, A. Aldaz, and J. M. Feliu, *Electrochim. Acta*, **54**, 4459 (2009).

[28] N. Hoshi, A. Nakahara, M. Nakamura, K. Sumitani, and O. Sakata, *Electrochim. Acta*, **53**, 6070 (2008).

[29] J. Souza-Garcia, C. A. Angelucci, V. Climent, and J. M. Feliu, *Electrochem. Commun.*, **34**, 291 (2013).

C Supplementary Information on Chapter 4

C.1 Formation Free Energy of Steps

In vacuum, the free energy required to form one unit length of an isolated step, f_{step}, is given by the temperature independent step formation energy, f^0_{step}, and an entropic term that accounts for the thermal fluctuation of steps due to the formation of kinks [1,2]:

$$f_{step}(T) = f^0_{step} - \frac{2\,k_B\,T}{a}\,exp(\frac{-f^0_{kink}}{k_B\,T}) \tag{C.1}$$

where a is the unit step length, k_B is the Boltzmann constant, T is the temperature, and f^0_{kink} is the formation energy of a kink. From this equation, it is evident that the presence of kinks decreases the free energy needed to form the step. Therefore, at any temperature greater than $T = 0$ K, the steps will never be completely straight, but they will present a certain roughness given by the concentration of kinks, which is determined by f^0_{kink} and T. The higher T or the lower f^0_{kink}, the higher the concentration of kinks and thus the cheaper in energy it is to form a step. Actually, at a certain T, the entropic term becomes large enough to counterbalance f^0_{step}, and hence f_{step} becomes zero.

It is noteworthy to mention also that f^0_{step} and f^0_{kink} depend on the step geometry. This is easy to realize for f^0_{step}, as (111) and (100) steps exhibit different microfacets with the lower terrace atoms. The geometric dependence of f^0_{kink} resides on the fact that creating a kink on a (111) step involves the formation of one unit length of a (100) step, while creating a kink on a (100) step involves the formation of one unit length of a (111) step.

In electrochemistry, however, the thermodynamic description of the step free energy becomes more complicated. Firstly because of the potential applied to the electrode, which adds a term to equation C.1. Secondly, because the species adsorbed at steps and kinks modify both $\eta(0)$ and ϵ_{kink}, and can favor one step geometry over the other (e.g. (100) steps over (111) steps) [3]. Nevertheless, the general concept is the same as in vacuum, and we can ensure that also in electrolyte the steps are not completely straight due to the presence of kinks.

C.2 H_{upd} Coverage

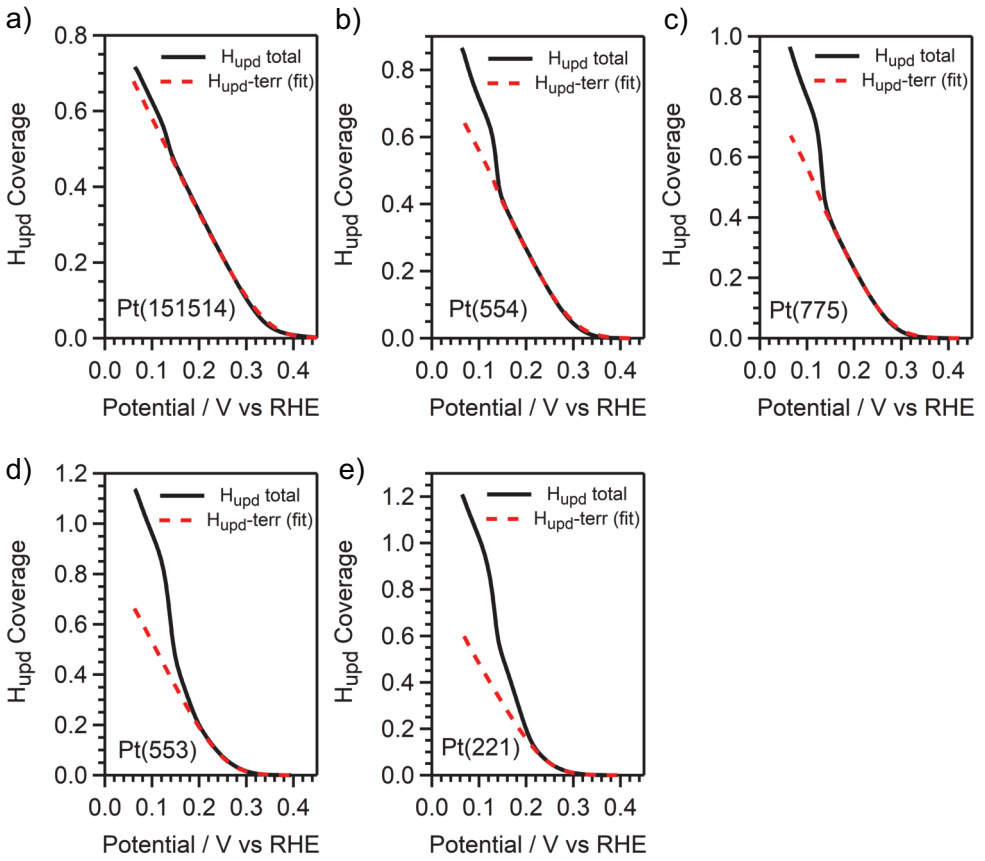

Figure C.1: Comparison of Total and Terrace H_{upd} Coverages. For each of the stepped surfaces studied (**a**-**e**), the H_{upd}-terrace coverage (in red) results from a fit of the terrace peak with the Frumkin isotherm, as explained in the main text. In all the cases the H_{upd}-terrace coverage matches well with the total H_{upd} coverage at potentials more positive than the (111) step peak.

C.3 Potential Limits for the Fitting of the PtOx Region

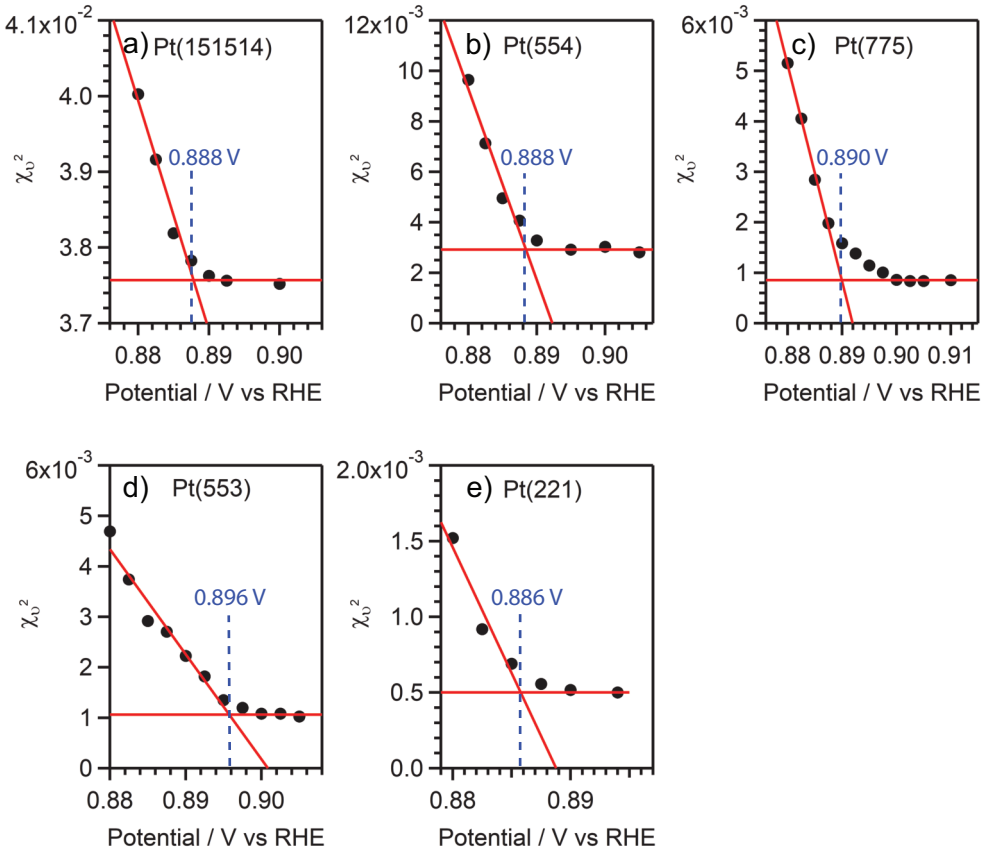

Figure C.2: Determination of the Lower Potential for Fitting the Platinum Oxidation Region. Normalized Chi Square values obtained from fitting the platinum oxidation region starting at the potentials indicated in the x axes. The upper potential was fixed at 1.09 V. The inflection point in the Normalized Chi Square values (marked with the dashed blue line) gives the lower potential used for the final fit.

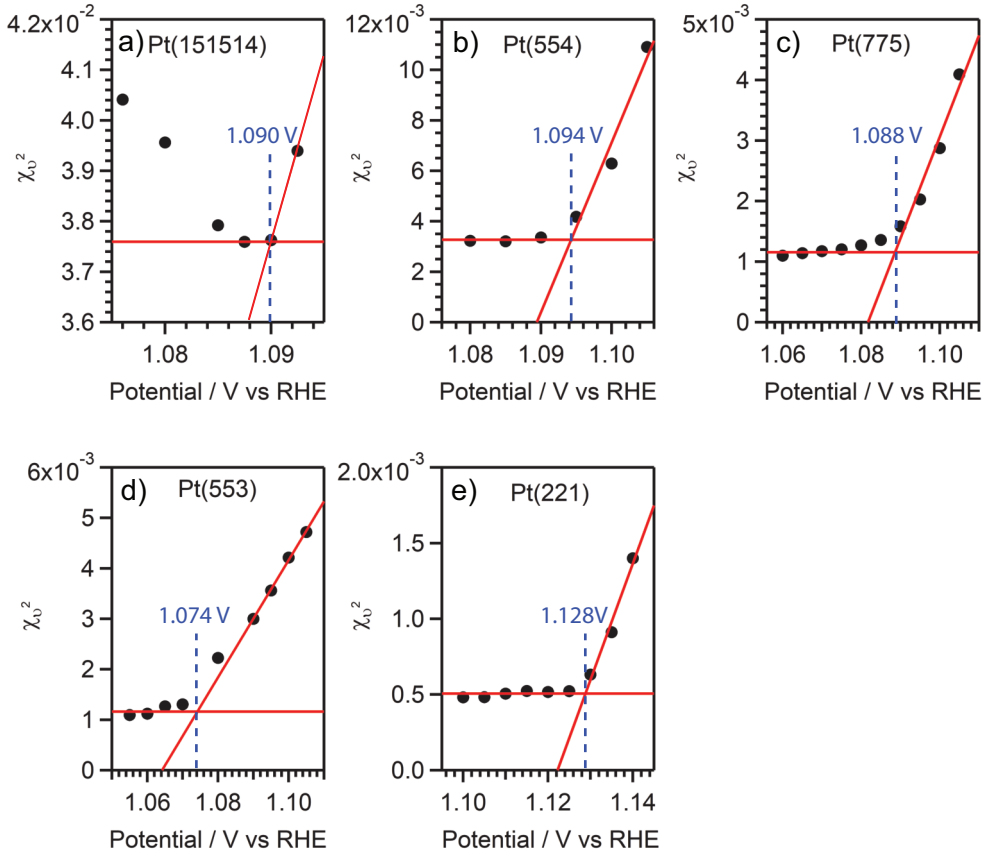

Figure C.3: Determination of the Upper Potential for Fitting the Platinum Oxidation Region. Normalized Chi Square values obtained from fitting the platinum oxidation region up to the potentials indicated in the x axes. The lower potential was fixed at 0.89 V. The inflection point in the Normalized Chi Square values (marked with the dashed blue line) gives the upper potential used for the final fit.

References

[1] H. Ibach, *Physics of Surfaces and Interfaces*, Springer, Amsterdam (2006).

[2] E. D. Williams and N. C. Bartelt, *Science*, **251**, 393 (1991).

[3] M. Kalff, G. Comsa, and T. Michely, *Phys. Rev. Lett.*, **81**, 1255 (1998).